POLITECNICO DI TORINO
Repository ISTITUZIONALE

Thermal effects on Common Rail injection system hydraulic performance

(Article begins on next page)

01 September 2025

Thermal effects on Common Rail injection system hydraulic performance

Alessandro Ferrari, Oscar Vento[(*)]

Energy Department, Politecnico di Torino, corso Duca degli Abruzzi 24, 10129, Torino, Italy

(*) Corresponding author. Email: oscar.vento@polito.it

1. Abstract

The effect of the fuel temperature on the hydraulic performance of a Common Rail diesel injector has been investigated with an integrated experimental-numerical approach. An experimental campaign pertaining to single and double injections has been performed for fuel tank temperatures ranging from 28°C to 68°C. In general, an augment in the injected mass has been observed for increasing values of the fuel tank temperature. Moreover, the interaction between the main and after injection changes with the temperature and the dwell time threshold for fusion-free injections increases with the fuel temperature. The temperature at the injector nozzle has been measured and compared with that obtained with a thermo-fluid dynamics simple model, showing that the real temperature and the estimated one correlate well. The influence of the fuel temperature on the internal injector dynamic has been explored by means of a validated 1D numerical model of the injector thermo-fluid dynamics. The main direct effect of the temperature variation concerns the needle lift, which reaches a larger peak value for a higher fuel temperature: this explains the general increment in the injected mass and the augmented value of the injection fusion threshold for the main-after injections. The obtained results could allow more accurate open-loop control strategies for the injected mass, which include thermal effects, to be implemented.

2. Introduction

The fuel injection apparatus has a key role in a powertrain, since engine efficiency [1], combustion [2] and pollutant emissions [3] are significantly influenced by the injection schedule and for this reason the injection system further development continues to be a research challenge even for alternative fuels.

The Common Rail (*CR*) fuel injection apparatus offers great flexibility in terms of number of injection events per engine cycle, dwell-times between shots and high injection pressure (up to 3000 bar) [4]. The designed shape and quantity of every fuel shot affect combustion and engine-out emission control [5]

29   and both design parameters, associated to the injector structure [6], and physical factors, such as the fuel

30   properties [7] or the ambient conditions [8], must be taken into account. Fractioning the injection quantity

31   between multiple shots with close-to-zero hydraulic dwell-times according to digital rate shaping

32   strategies, can allow combustion noise to be reduced significantly [9]. An ultra-high injection pressure

33   coupled with small injection holes allow optimal level of fuel atomization, mixture homogeneity and

34   easy evaporation [10]. Soot and hydrocarbon (*HC*) emission reduction can be obtained, thanks to the

35   diminished liquid length and the consequent reduced impingement on walls, and it can be coupled with

36   a NO_x decrease if high EGR rates are simultaneously applied [11]. Besides, an optimal number of orifices

37   and an ideal angular position of them in the nozzle are able to affect the inter- and near-nozzle flow

38   patterns, thus positively affecting lift-off flame and jet interaction with the squish regions [12].

39   By investigating the influence of low temperature (for both the fuel and the injector body) it has been

40   seen that an injector equipped with a pressure balanced valve shows a pronounced reduction of the fuel

41   injected quantity under cold conditions (the reference temperature was 40 °C for the fuel and 90 °C for

42   the injector body) while a three-way valve injector features negligible differences in the injected mass at

43   800 bar of rail pressure and a progressive increment of the fuel quantity delivered beyond this rail

44   pressure level [13].

45   The effect of the injected fuel temperature has been analysed with reference to the spray development

46   and the combustion evolution. For both diesel fuel and DME (dimethyl ether), the higher is the fuel

47   temperature, the earlier is the evaporation and the lower the fuel plume penetration. This causes a lower

48   maximum combustion pressure and a more delayed start of combustion: both these effects lead to a

49   reduction in the NO_x emissions [14, 15]. Furthermore, a reduction in the fuel temperature can cause a

50   higher non-uniformity degree in the fuel-air mixture, which can increase the time necessary to reach a

51   constant level of evaporation rate and can lead to augmented emissions in unburned *HC* [16]. A

52   significant sensitivity of fuel economy and NO_x emission level to the fuel temperature at the injector

53   nozzle has been noticed even for a biodiesel fuelled engine, especially if low EGR rate is used [17].

54   When a pure biodiesel (B100), characterized by a high viscosity, is considered, the injected fuel

55   temperature can become crucial to improve the biodiesel spray performance. In fact, an increase in the

56   fuel temperature enlarges the spray angle cone and the spray area, which are usually smaller at a fixed

57   temperature if compared with normal diesel fuel. Furthermore, even the pump efficiency improves, due

58   to the reduced viscous friction loses, since fuel viscosity reduces with fuel temperature [18].

59   The flow through the injection system circuit is not isothermal. The major source of heat input to the fuel

60   in the tank during system working is the fuel recirculated from the injectors [19]. The fuel in the tank

61   reaches the injector inlet after the pumping phase, which determines a temperature increment of about 1

62   °C every 100 bar of compression [20]. Concerning the temperature evolution within the injector, it has

63   been often predicted in the literature with an isothermal flow assumption [21, 22]. However, with this

64   hypothesis, the temperature rise, due to the viscous dissipation through the injector restrictions and due

65   to the pressure drop, is not simulated [23]. The variations in density, viscosity [21] and bulk modulus

66   [24] with temperature can affect the injector behaviour. In a ballistic injector, where the needle never

67   reaches the upper stroke-end under the usual operating conditions [25], the needle dynamics significantly

68   depends on the pressure and viscous forces which are affected by the temperature [26]. As far as the

69   nozzle holes are concerned, a complex temperature pattern can be identified with 3D numerical

70   simulation, and a separated behaviour between the boundary layer and the core flow is often highlighted.

71   If a 2000 bar injection is considered, the maximum temperature difference in the flow can reach 80 °C

72   between the fluid at the core region and the one at the walls, which is a remarkable value if the

73   temperature dependence of the fuel properties is taken into account [27]. All this highlights a significant

74   role of thermal aspects in the hydraulic performance with effects on the spray.

75   In the present work, temperature effects on the injector working are analysed. With regard to the

76   hydraulic performance, the temperature at the injector nozzle hole exit has been measured and compared

77   with the one obtained by means of a simple thermodynamic model. Furthermore, a 1D numerical model

78   has been employed to investigate the injector internal dynamics dependence on the fuel temperature.

79   Numerical and experimental tests on single and double injections have been considered in a wide range

80   of nominal rail pressures under different values of the fuel temperature in the tank.

81 ## 3. **Experimental facility**

82   Experimental tests were performed in the Internal Combustion Engines Laboratory at the Politecnico di

83   Torino by means of the Moehwald-Bosch hydraulic test bench for fuel injection systems (maximum

84   speed: 6100 rpm, maximum torque: 100 Nm, nominal power: 35 kW).

85   The selected calibration fluid is the Shell V-Oil 1404 (ISO 4113) since it is capable to satisfactorily

86   reproduce diesel oil properties up to 150 °C over the entire pressure range.

87   Tests were conducted on a Bosch CR injection system for a 4 cylinders passenger car diesel engine. A

88   high-pressure rotary pump, featuring a displacement of 430 mm^3/rev and a double effect single piston, is

89   employed to feed the rail. The rail is connected with solenoid-actuated CRI 2.18 injectors, a scheme of

90   which is reported in Fig. 1. The high-pressure fuel enters the injector and a part of it reaches the delivery

91   chamber (volume V_{dc}) upstream the nozzle zone, and the other part, through the Z hole, fills the control

92   chamber (volume V_{cc}). As soon as the electrical current supplied by the Electronic Control Unit (ECU)

93   is switched on, the injector solenoid is energized and the control chamber discharges fuel from the pilot

94   valve through the A hole. Therefore, the pressure forces acting on the needle become unbalanced and the

95   latter moves up, opening the nozzle and allowing the fuel injection. When the ECU switches off the

96   current to the solenoid, the closure of the pilot valve makes the pressure rise in the control chamber,

97   therefore the needle starts its closure phase, which finishes when its tip touches the seat. Hence, the

98   nozzle is again closed and injection ends [9]. The injected fuel quantity depends on both the time-

99   averaged value of the injection pressure and on the hydraulic duration of the injection, which is related

100   to the electrical command to the solenoid, i.e. the energizing time (*ET*) [28].
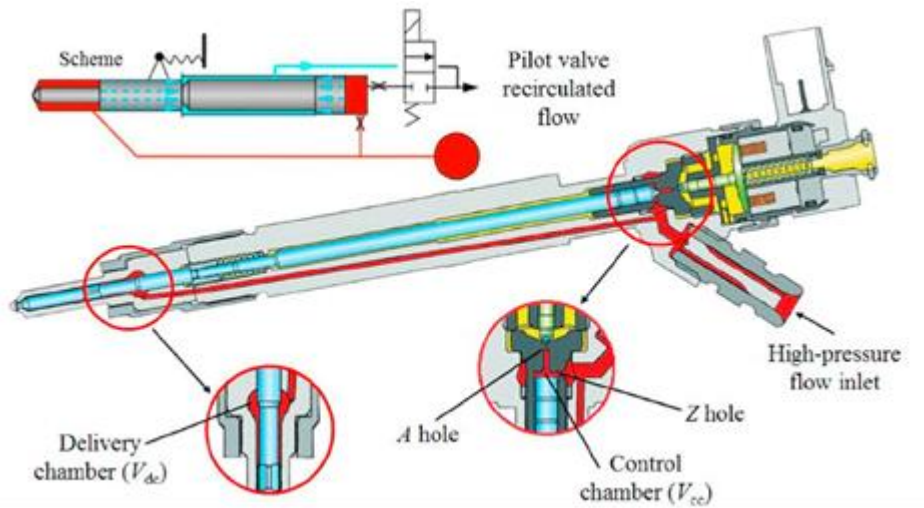

101

102   **Figure 1. CRI 2.18 injector.**

103

104   A piezoresistive transducer has been mounted at the injector inlet along the rail-to-injector pipe to

105   measure the pressure time history ($p_{inj,in}$) and this datum will be used as a boundary condition for the

106   numerical model. The transducer measuring range is up to 2000 bar and its linearity error is lower than

107   ±0.1% of the fuel scale value. It has been assumed that the only uncertainty contribution that affects the

108   transducer accuracy is the linearity error, which is lower than ±2 bar.

109   The injected flow-rate and the injected mass have been measured by means of the HDA flowmeter. In

110   this instrument the pressure in a closed volume is measured, together with the speed of sound (for which

111   an ultrasonic sensor is employed), then, by following Zeuch's method, the injected mass flow-rate is

112   obtained [29].

113   The fuel temperature at the nozzle hole exit has been measured by means of a PT100 temperature sensor

114   mounted at a distance of 25 mm from the injector tip along a duct with a counterpressure of 40 bar where

115   the fuel is injected. The same injector previously mounted in the HDA to detect the injected flow-rate

116   has then been made inject the fuel in the pipe with the PT100 sensor to measure the fuel temperature

117   under the same controlled working conditions.

118   Single injections, together with pilot-main and main-after injections, have been considered in this

119   research investigation. Tests have been performed by varying the *ET* at different nominal rail pressure

120   (p_{nom}) values for single injections, while for double injections the *ET* values for the considered injections

121   have been kept constant and the dwell time between the shots has been varied. The fuel temperature at

122   the pump inlet was varied from 28 °C to 68 °C. In particular, 28°C represents the minimum value that

123   can be controlled by the current test bench, 40 °C is usually assumed as the reference temperature for

124   hydraulic tests by the fuel injection system manufacturers and 68 °C represents the maximum

125   temperature that can be reached on the test bench for safety reasons. The hydraulic test bench can heat

126   the fuel in the tank by means of a heating coil and, at the pump inlet, the fuel temperature is controlled

127   by means of a heat exchanger where the cooling water flowrate is regulated in order to fulfil the fuel

128   temperature requirement (the fuel temperature at the pump inlet is measured by means of a temperature

129   probe that represents the feedback signal to modify the cooling water flowrate). Tests have been

130   performed at a pump speed of 2000 rpm.

131   ## 4. **Fuel properties and temperature in the injection apparatus**

132   The temperature can affect the fuel properties significantly. The ones here considered are the density (ρ),

133   the bulk modulus (E), the dynamic viscosity (μ) and the thermal expansivity (β), which is defined as

134    $-\frac{1}{\rho}\left(\frac{\partial \rho}{\partial T}\right)_p$. Figure 2 reports the trends of the ISO 4113 oil properties, experimentally determined, as

135   functions of the temperature for different nominal rail pressures, according to [21]: symbols stand for the

136   experimental values, whereas the solid lines correspond to the determined polynomial interpolating

137   expressions.

138   The test rig can control the tank oil temperature (T_{tank}). By assuming an isentropic evolution of the fuel

139   through the pump compression, the temperature increase, due to the pressure rise, can be estimated.

140   If the fundamental thermodynamic state relation [30] is considered for an isentropic compression, one

141   has:

$$dh = \frac{dp}{\rho} \qquad (1)$$

143   where h is the enthalpy per unit of mass. For a liquid, the enthalpy is defined as:

$$dh = c_p dT + (1 - \beta T)\frac{dp}{\rho} \qquad (2)$$

145   where c_p is the specific heat at constant pressure. By combining Eqs. (1) and (2), one obtains:
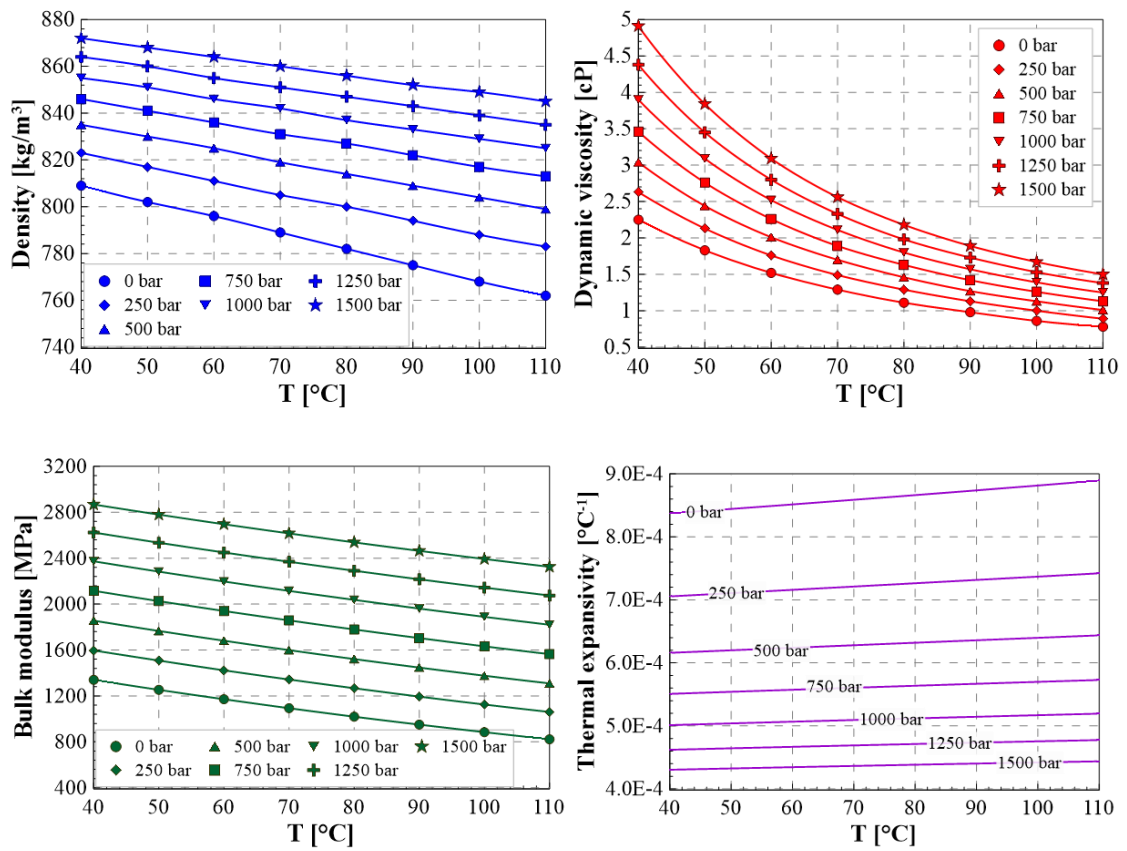
$$c_p dT = \beta T \frac{dp}{\rho} \qquad (3)$$

147

148   **Figure 2. ISO 4113 oil properties with respect temperature and pressure.**
149

150   Hence an estimation of the temperature level in the high-pressure circuit can be obtained for a certain

151   nominal rail pressure.

152   The fuel temperature through the injector can be estimated by considering an isenthalpic evolution [21],

153   if the injector is roughly regarded as a set of localized restrictors. The injected fuel temperature can

154   therefore be predicted as follows:

$$c_p dT = (\beta T - 1)\frac{dp}{\rho} \qquad (4)$$

6

5. <u>Experimental results</u>

Figure 3 reports the trend of the fuel temperature measured at the nozzle hole exit with respect to ET; data refers to p_{nom}= 800 bar and to both T_{tank}= 40 °C and T_{tank}= 68 °C. Tests were also performed at T_{tank}= 28°C and measure fuel temperatures resulted slightly lower than the corresponding ones at T_{tank}= 40 °C. After a certain value of ET, the measured temperature reaches an asymptotic value. This can be interpreted by considering the measuring procedure used to obtain the temperature value. When ET is small, the injected flow-rate is not high enough to let the sensor measure a steady-state temperature in the pipe where the fuel is injected. Therefore, if the ET is increased, the detected temperature augments and finally reaches an asymptotic value, which is the steady-state one that should be considered in the comparison with the isenthalpic model. The asymptotic values measured for different nominal rail pressures (cf. Fig. 3) have been adopted as the fuel temperatures at the nozzle outlet in the numerical simulations.

In Fig. 4, the measured oil temperature at the nozzle exit for ET=3000 μs is plotted (with symbols) with respect to the correspondent isenthalpic temperature obtained for a certain rail pressure under the adiabatic assumption, for both T_{tank} = 40 °C and T_{tank} = 68 °C. Although the curves are well distinct from the bisector and the isenthalpic assumption overestimates the real temperature (the injector is less dissipative than a restrictor) the estimations provided can be reasonable. Furthermore, the experimental and isenthalpic temperatures are well correlated, and the correlation is almost linear (cf. the continuous lines in Fig. 4). Hence, for a fixed T_{tank} and a given rail pressure level, the isenthalpic temperature at the nozzle can be obtained by means of Eq. (4) and a more accurate estimation of the real temperature can be obtained by means of a correlation curve which can be determined for each injector typology.
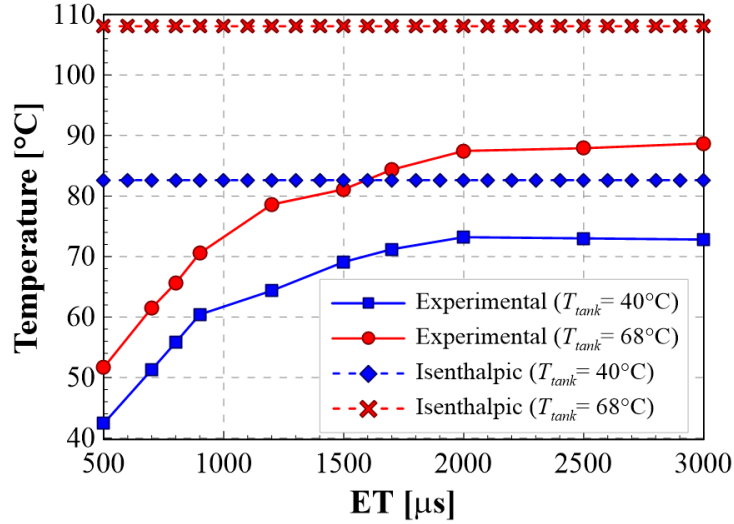
Figure 3. Fuel temperature at the injector exit for different ET and T_{tank} values (p_{nom} = 800 bar).
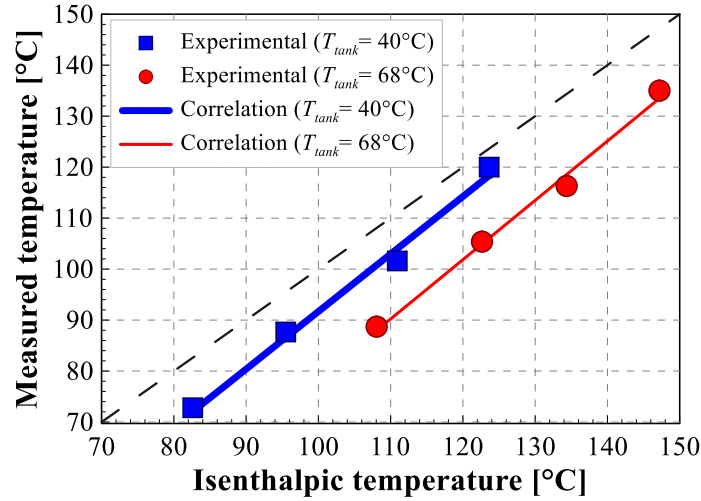

Figure 4. Correlation between the measured temperature at the injector outlet and the isenthalpic temperature.

Tests for single injections have been performed over a wide range of nominal rail pressure (between 600

bar and 1800 bar) and of *ET* (between 350 µs and 1000 µs) in order to explore the entire range of working

conditions for a diesel passenger car. Figure 5 shows the injector characteristics pertaining to different

nominal rail pressure levels and to two distinct fuel tank temperatures, namely 40 °C and

68 °C. As can be inferred from Fig. 5, the injected mass generally increases with the fuel temperature for

a fixed working condition in terms of p_{nom} and *ET*.

Figure 6 reports the injected flow-rates for p_{nom}=1600 bar and *ET*= 600 µs, at two different T_{tank} values.

It can be observed that the injection temporal length (*ITL*) increases with the tank fuel temperature, and

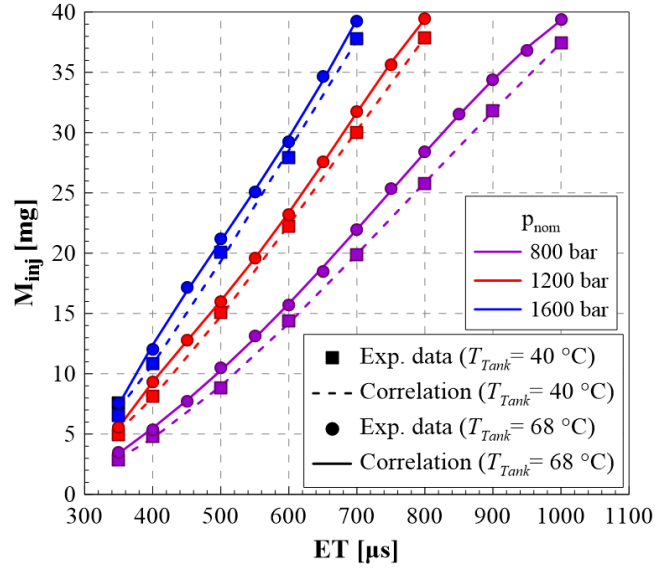this leads to an augmented injected fuel quantity for fixed *ET* and p_{nom}. [31].

Figure 5. Injector characteristics for different nominal rail pressure levels and fuel tank temperatures.
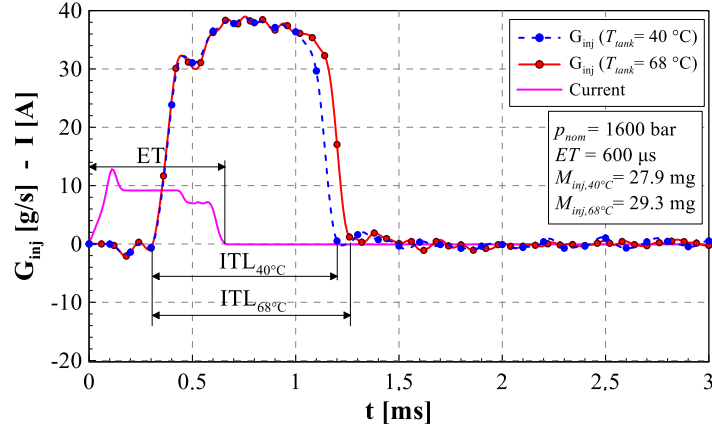

Figure 6. Injected flow-rate for different fuel tank temperature values (pnom = 1600 bar, ET = 600 µs).

As far as the double injections experimental campaign is concerned, a CRI 2.20 injector has been employed. This injector, differently from the CRI 2.18 used for the analysis on single injections, features a Minirail in place of the delivery chamber (the latter corresponds to volume V_{dc} in Fig. 1) in order to reduce the injected mass fluctuation of the second shot with respect to the dwell time [25]. It has been already verified that also the CRI 2.20 injector is affected by a thermal drift similar that of the CRI 2.18 injector, and an augment in the injected mass can be detected as the fuel temperature increases [31]. Pertaining to pilot-main injections, a DT sweep has been reported in Fig. 7, referring to p_{nom} = 800 bar, ET_{pil} = 230 µs and ET_{main} = 500 µs. The overall injected mass $M_{inj,total}$ (given by the sum of pilot and main injected masses), measured by means of the HDA, has been reported at different DT values for both T_{tank} = 40°C (blue curve) and T_{tank} = 68°C (red curve). The injected mass increases with the temperature, as

209 occurs for single injections, while the dynamic features of the system, such as the injection fusion

210 threshold, do not vary appreciably.

211 Regarding main-after injections, the overall injected mass with respect to the dwell time value is

212 represented in Figure 8 for the case p_{nom} = 1400 bar, ET_{main} = 400 µs, ET_{aft} = 200 µs at two different fuel

213 tank temperatures, i.e. T_{tank} = 40°C (blue curve) and T_{tank} = 68°C (red curve). The most evident effect is,

214 even in this case, an augment in the injected mass when the fuel temperature increases. Moreover, it can

215 be observed that the injection fusion threshold, that is the minimum dwell-time value for which two

216 injections are still hydraulically distinct, increases with the temperature. This is obvious in Figure 9,

217 where the injected flowrates for the DT = 540 µs case is reported for both T_{tank} = 40°C (blue curve, the

218 main and after injection are still separated), and T_{tank} = 68 °C, (red curve, where the needle never closes

219 the nozzle holes during the entire injection event).

220 Many strategies can be implemented on the ECU to correct the injection schedules in order to compensate

221 for the abovementioned fuel temperature effects. As an example, the main energizing time can be

222 modified according to the engine water cooling temperature, by means of on an open-loop strategy,

223 through an empirical coefficient. The presented thermo-fluid dynamic model allows the temperature of

224 the injected fuel, which considers the temperature increase due to both the fuel compression in the high-

225 pressure pump and the fuel expansion across the injector, to be used to refine the open-loop control
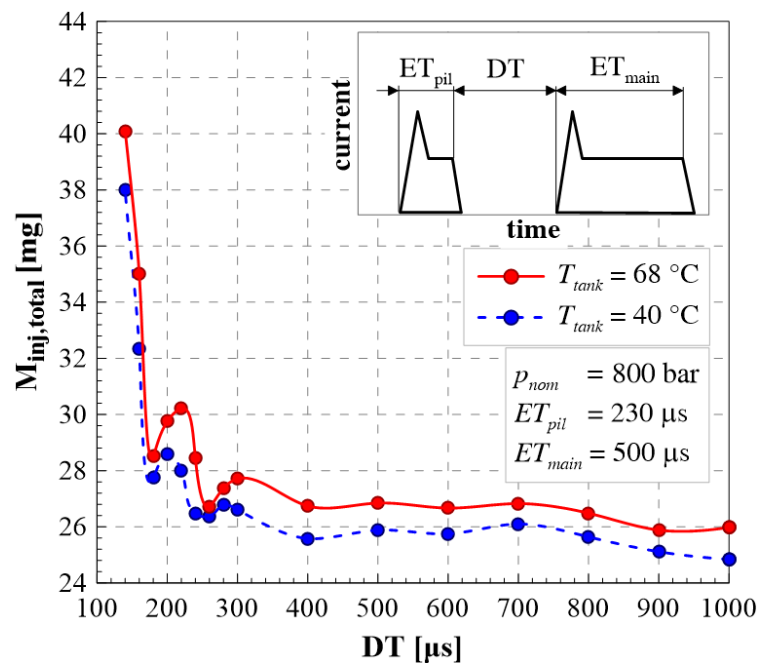
226 strategy of the injected mass.

227

228 **Figure 7. Pilot-main injection *DT* sweep for different fuel tank temperatures.**
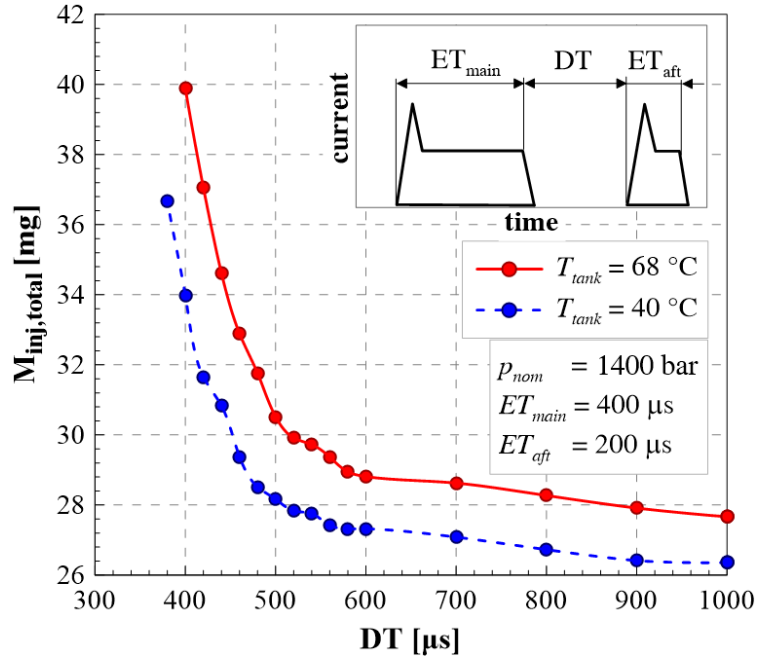
229

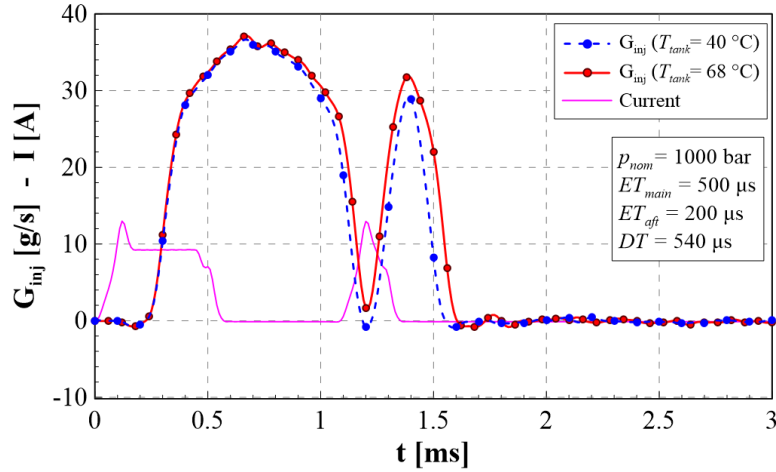Figure 8. Main-after injection *DT* sweep for different fuel tank temperatures.

Figure 9. Injected flow-rate for a main-after injection for different fuel tank temperatures.

6. Model description

The analysis regarding single injection is based on a 1D injector numerical diagnostic tool developed in

[32, 33] and further validated at different fuel temperatures. A scheme of the 1D model is represented in

Fig. 10. The circuit generally consists of a network of 0D chambers connected by means of 1D pipes

[34]. The boundary conditions consist of the measured pressure time history at the injector inlet along

the rail-to-injector pipe and of the electrical current signal provided to the solenoid of the pilot valve. By

selecting these boundary conditions, any inaccuracy, due to the modelling of the rail, the injector feeding

pipe, the pump and the ECU, can be avoided.

11

244   During the needle movement, a viscous force is generated between the needle and the injector body, due

245   to the presence of a thin boundary layer. The flow in the small annular passage (cf. Fig. 10) is laminar

246   and follows Poiseuille's law. The viscous friction force in this zone can therefore be evaluated as [35]:

247    $$F_{fric} = \frac{\mu \cdot L_c \cdot v \cdot \pi \cdot d_n}{\delta_r} \qquad (5)$$

248   where d_n is the needle diameter, L_c represents the length of the annular passage, δ_r is the radial distance

249   between the needle and the injector holder and v is the velocity of the needle.

250   The needle movement is related to the pressure variation in the control chamber, that is to the control

251   chamber discharge and refilling through the A and Z holes, respectively (cf. Fig. 10). The Z hole is in a

252   non-cavitating condition, whereas the A hole can experience cavitation conditions [36]. One important

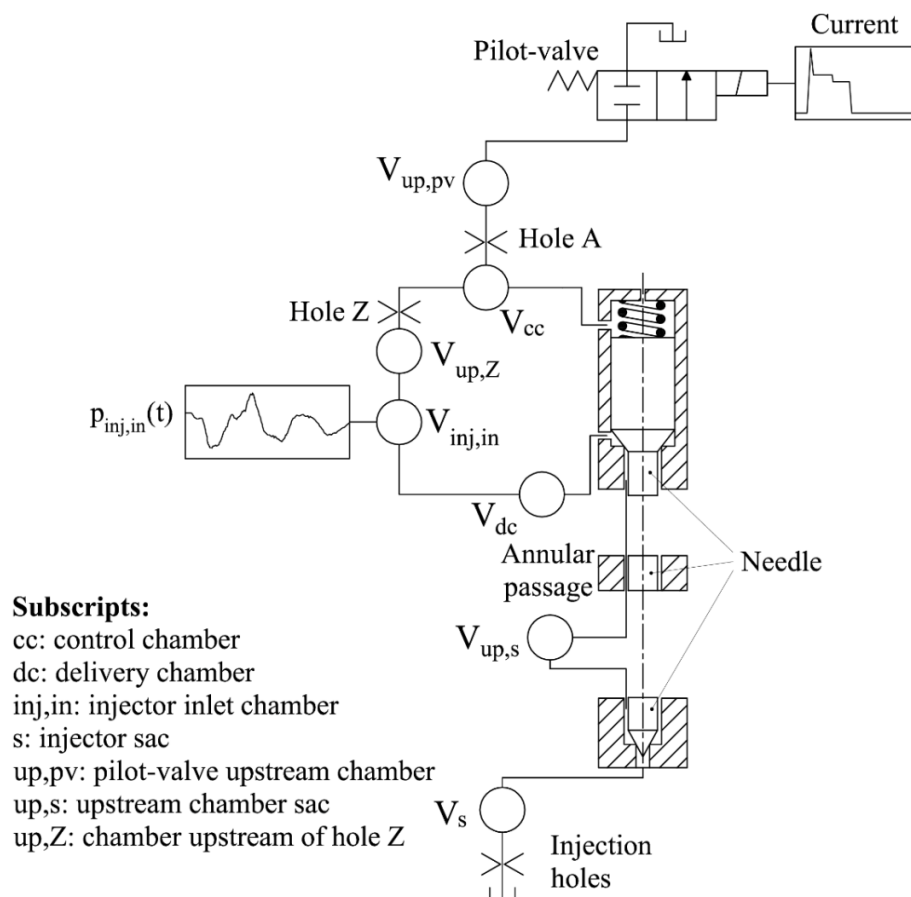253   point in thermal models concerns the discharge coefficient of the holes.

254

256   **Figure 10. Scheme of the 1D numerical model.**

257

258   The discharge coefficient of a hole is defined as the ratio of the effective flow-rate to the ideal one,

259   obtained by means of the Bernoulli equation for a liquid flow [37].

260 For a cavitation-free hole the discharge coefficient C_d has been defined as follows [38]:

$$C_d = C_{d,max} \cdot tanh\left(\frac{2 \cdot Re}{Re_{crit}}\right) \qquad (6)$$

262 where $C_{d,max}$ is the maximum value of the discharge coefficient, Re is the Reynolds number and Re_{crit}

263 is the critical Reynolds number, where the transition between laminar and turbulent flow occurs. The

264 Reynolds number is calculated in the following way:

$$Re = \frac{D}{\mu} \cdot \sqrt{2\Delta p \rho} \qquad (7)$$

266 where D is the hole diameter and Δp the pressure drop across the hole.

267 When the flow through the hole can be subjected to cavitation phenomena, the cavitation number CN can

268 be introduced [39]:

$$CN = \frac{p_{in} - p_v}{p_{in} - p_{out}} \qquad (8)$$

270 where p_{in}, p_{out} and p_v are the pressure value at the inlet of the hole, at the outlet of the hole and the

271 vapour pressure of the fuel, respectively. When CN is lower than a critical cavitation number (CN_{crit})

272 which is experimentally obtained, cavitation occurs, and the discharge coefficient is calculated by

273 considering the actual cavitation number CN and the contraction coefficient C_c according to this

274 expression [40]:

$$C_d = C_c \cdot \sqrt{CN} \qquad (9)$$

276 In the present investigation, the flow coefficient pertaining to Z hole was evaluated with Eqs. (6) and

277 (7), whereas the complete model of C_d which includes Eqs. (6-9) was implemented for A hole and for

278 the injection holes in order to simulate possible cavitation occurrences.

6.1 <u>Numerical model results</u>

280 Figure 11 shows the comparison between the experimental injected flow-rates (plotted with symbols)

281 and the numerical ones (plotted with continuous line) for the two pressure levels 800 bar (Fig. 11a), and

282 1700 bar (Fig. 11b). The T_{tank} was set at 40°C and the results pertaining to different ETs have been

283 reported in the plots. The corresponding results referring to $T_{tank} = 68$ °C have been plotted in Fig. 12. It

284 can be observed that the numerical results match the experimental ones accurately.

285 In Fig. 13, the numerical control chamber pressure traces have been reported for both $T_{tank} = 40$ °C and

286 $T_{tank} = 68$ °C ($p_{nom} = 800$ bar and $ET = 800$ µs). As can be inferred, the difference in fuel temperature does

287 not affect significantly the pressure time history in the control chamber because both the flow-rates

288   through the Z and A holes are almost the same for the two cases. This is in line with the results available

289   in the literature, where the effect of the fuel temperature on the control chamber pressure and flow-rates

290   through A and Z holes are significant only when the fuel temperature within the injector is below 0° C

291   [36]. From the numerical model it results that the A hole is experiencing cavitating condition for both

292   the tested T_{tank} temperatures and only a small increase in the CN can be noticed for $T_{tank} = 40°C$, leading

293   to a slight augment in the C_d value. Instead, the Z hole doesn't undergo any cavitating regime and the

294   flow is turbulent for both $T_{tank} = 40°C$ and $T_{tank} = 68 °C$.

295   Figure 14 reports the numerical pressure time histories detected in the delivery chamber (p_{dc}), in the

296   upstream-sac chamber ($p_{up,s}$) and in the injector sac (p_{sac}) (cf. Fig. 10 for the chambers location), as well
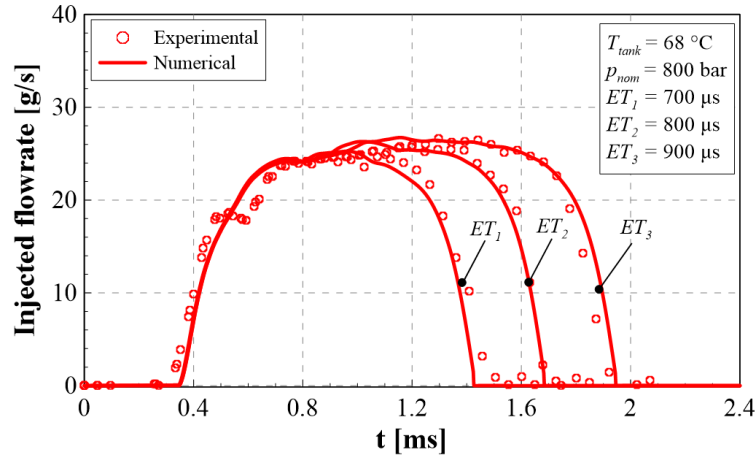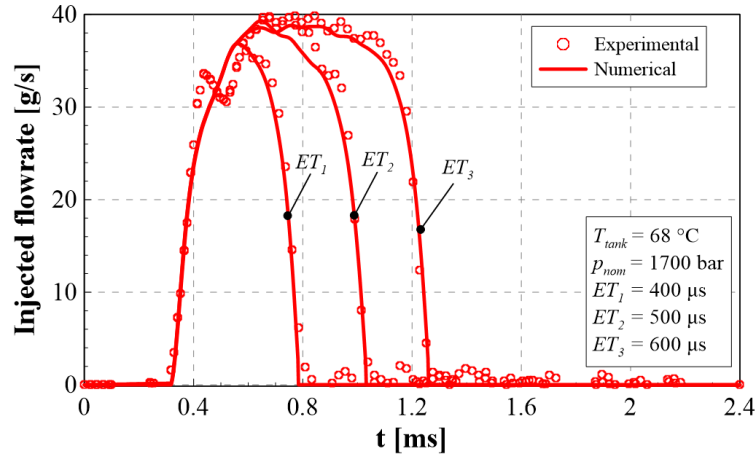
297

298

299   **(a)**

300
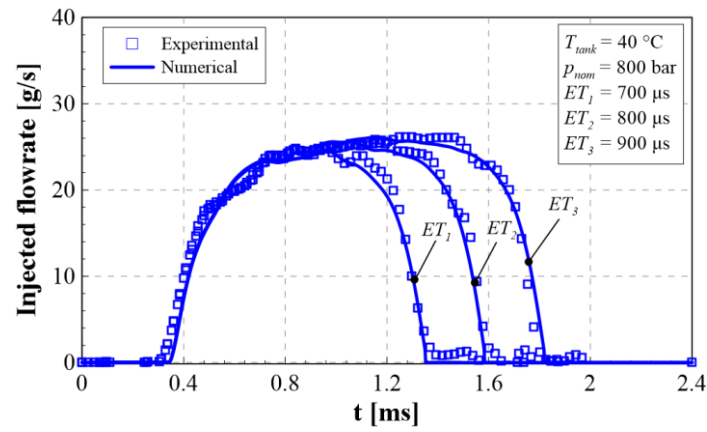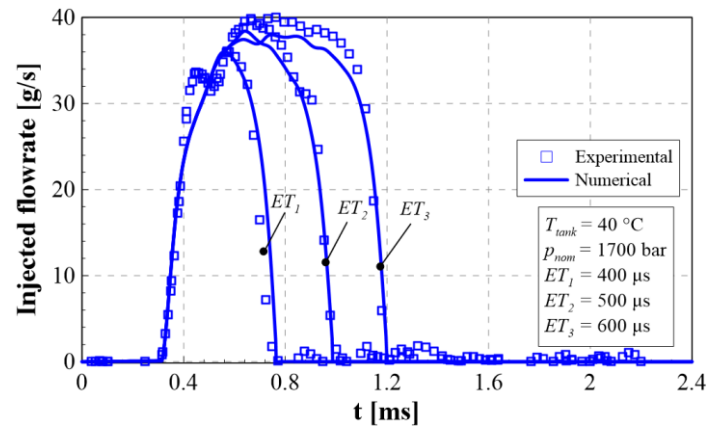
301   **(b)**
302   **Figure 11. Experimental injected flow-rates compared with the numerical ones with $T_{tank} = 40 °C$,**
303   **$p_{nom} = 800$ bar (a), $p_{nom} = 1700$ bar (b).**
304   as the needle lift numerical trace (p_{nom}=800 bar, ET=1000 us, T_{tank}=40 °C). The temperature at the injector

305   inlet (cf. $V_{inj,in}$ in Fig. 10) is provided as an input datum to the injector model and has been obtained by

306   means of Eq. (3). For the other injector chambers, starting from the injector inlet temperature, the

14

307　instantaneous pressure difference between two adjacent chambers (cf. $\Delta p_{dc \rightarrow up,s}$, $\Delta p_{up,s \rightarrow sac}$ and $\Delta p_{sac \rightarrow cyl}$

308　in Fig. 14) is used to estimate the temperature rise under the $h{=}const$ hypothesis

309　and, by means of the correlation reported in Fig. 4, an estimation of the real temperature can be obtained.

310　If the isenthalpic temperature results to be outside from the considered range in Fig. 4, a linear

311　extrapolation has been performed. In fact, based on data of fuel temperature measured at the nozzle exit

312　for a wide range of p_{nom} values in [41], it was possible to extend the linear correlations reported in Fig. 4

313　up to about 160 °C (for T_{tank}= 40 °C) and to about 180 °C (for T_{tank}= 68 °C).

314

315

(a)

316

317

(b)

318　**Figure 12. Experimental injected flow-rates compared with the numerical ones with with T_{tank} = 68 °C,**
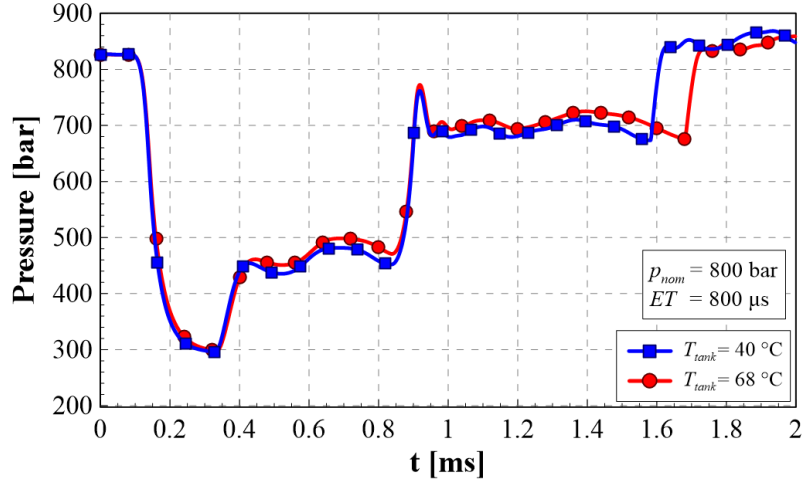319　**p_{nom} = 800 bar (a), p_{nom} = 1700 bar (b).**
320

**Figure 13. Pressure in the control chamber for T_{tank} = 40 °C and 68 °C,
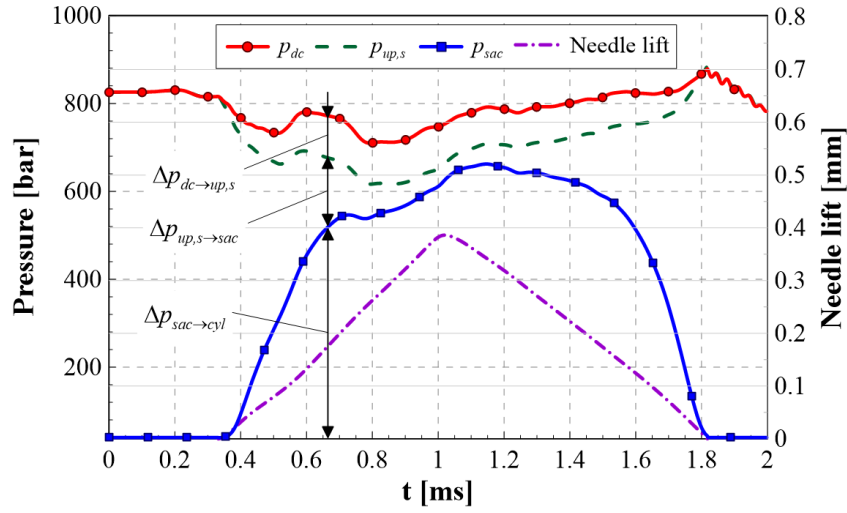p_{nom} = 800 bar, ET= 800 µs .**

**Figure 14. Pressure time histories and needle lift from the numerical model, p_{nom} = 800 bar, ET= 800 µs,
T_{tank} = 40 °C.**

At the beginning and at the end of the injection event, the pressure drop $\Delta p_{up,s \to sac}$ is larger than $\Delta p_{sac \to cyl}$

(cf. Fig. 14) because the restricted flow area is at the needle-seat passage. Therefore, the fuel heating

phase mainly occurs when the fuel flows across the passage between the needle and its seat. On the other

hand, when the needle lift is sufficiently high and the flow-rate is controlled by the nozzle holes, $\Delta p_{sac \to cyl}$

becomes much larger than $\Delta p_{up,s \to sac}$, hence the fuel heating mainly occurs through the nozzle holes.

In Fig. 15 the numerical needle lift time distribution is reported, for both the considered T_{tank}

temperatures, together with the numerical injected flow-rates (p_{nom} = 800 bar, ET = 800 µs). Figure 16

plots the same quantities as in Fig. 15 but with reference to a different working condition (p_{nom} = 1700
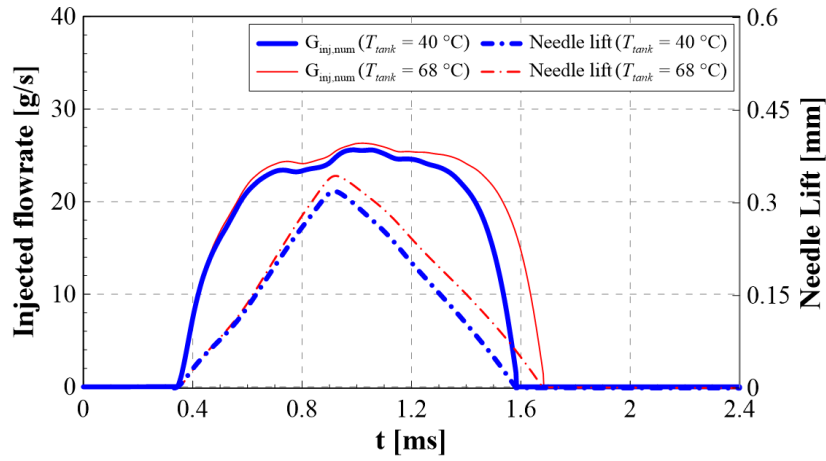
bar, ET = 600 µs).

16

Figure 15. Injected flowrate and needle lift for T_{tank} = 40 °C and 68 °C, p_{nom} = 800 bar, ET = 800 µs .
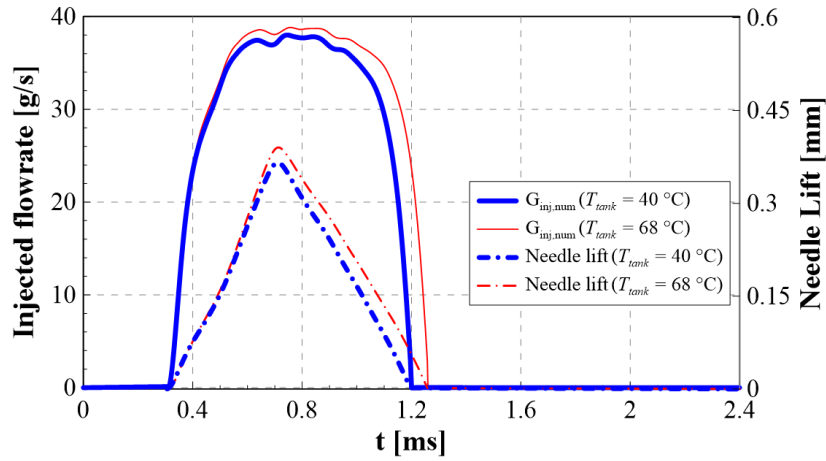
Figure 16. Injected flowrate and needle lift for T_{tank} = 40 °C and 68 °C, p_{nom} = 1700 bar, ET = 600 µs .
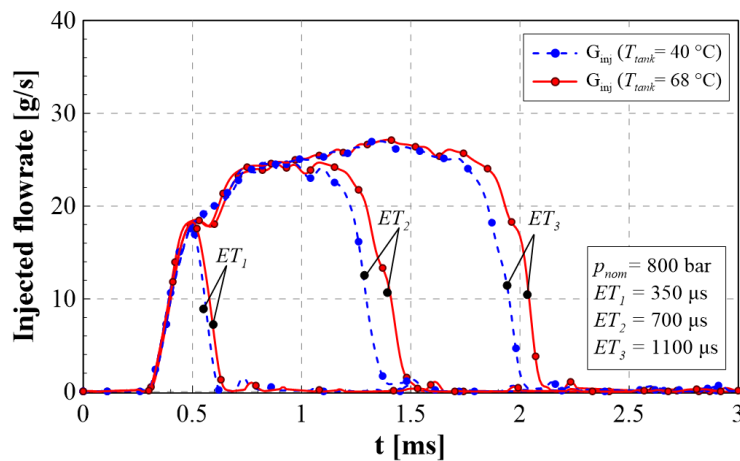
Figure 17. Injected flow-rates for different ET values with T_{tank} = 40 °C and 68 °C, p_{nom} = 800 bar.

In general, since the fuel viscosity reduces with the temperature (the decreasing trend is exponential in

Fig. 2), the viscous force acting on the needle diminishes as the fuel temperature augments. Therefore,

17

due to the reduced viscous force, the needle velocity increases during the opening phase as T_{tank} augments, leading to a higher needle peak lift value under a fixed ET. Then, after the electrical current is switched off, the needle starts its closure phase and, the higher is the temperature, the larger is the needle downstroke required to close the nozzle, and therefore the longer are the nozzle closure delay and the injection duration.

The effect of the fuel temperature is less obvious for injections characterized by small ETs, as is shown in Fig. 17. In fact, a shorter-ET injection is characterized by a smaller needle lift peak value and the absolute variation of the latter with T_{tank} is small. Hence, the higher is the needle lift peak value, the more evident is the effect of the fuel temperature in the final part of the injected flow-rate.

In [36] it has been verified that, even for a CRI 2.20 injector, the main effect of the fuel temperature, in the considered range, is given by a reduced viscous force acting on the needle, which leads to a higher needle lift peak. Therefore, for the pilot-main injections, the higher needle lift peak obtained at higher fuel temperature leads to a general increment in the mass, although the injection fusion threshold does not change considerably, as shown in Fig. 7. Instead, for main-after injections, when the tank fuel temperature grows, an augment in the injection fusion threshold can be detected, together with an increment in the injected mass (cf. Figs. 8-9). The injection fusion threshold increment is justified, since the tendency to reach higher needle-lift peak values for larger fuel temperatures becomes more evident for longer injections (cf. Fig 17): unlike pilot-main schedules, the shot with the larger ET is the former in main-after injections.

7. Conclusions

The fuel temperature effect on the hydraulic performance of a CR injection system has been analyzed by means of both experimental and numerical results. The major findings can be summarized as follows:

- the experimental campaign on single and double injections (pilot-main and main-after schedules) has shown that, when the fuel temperature increases, the injected mass generally grows. Furthermore, the fuel temperature appreciably affects the injection fusion threshold of the main-after injections;

- the injected fuel temperature has been measured along a pipe where the fuel is injected, at a distance of 25 mm from the injector tip. This experimental temperature has been compared successfully with the one obtained by means of a newly developed simple thermo-fluid dynamics model: starting from the fuel tank temperature, and by considering an isentropic compression through the pump, the fuel temperature

18

380 at the injector entrance has been obtained. Furthermore, by means of an isenthalpic evolution assumption

381 across the injector, the final temperature at the nozzle exit has been calculated;

382 - a 1D numerical model has been used to investigate the injector dynamics at different fuel temperatures.

383 The most relevant effect of the fuel temperature increase is the reduction in the fuel viscosity, which

384 leads to a diminished viscous force that acts against the needle movement. When the fuel temperature

385 increases, the needle reaches an augmented peak value, which explains the experimental differences with

386 respect to the fuel temperature for both single and double injections;

387 - the 1D numerical model shows that the fuel heating inside the injector occurs primarily in

388 correspondence of the needle seat passage, with an effect on the beginning and end of the injection law,

389 as well as across the nozzle holes with an effect on the central part of the injection law;

390 - an innovative open-loop control strategy of the injected mass, based on the estimated nozzle exit fuel

391 temperature, could be designed to improve the compensation of the injector thermal drifts during engine

392 operation (the current strategies are usually based on the water cooling temperature).

393 **8. <u>References</u>**

394 [1] Beatrice, C., Di Blasio, G., Pesce, F.C., Vassallo, A. et al., "Key Fuel Injection System Features for

395 Efficiency Improvement in Future Diesel Passenger Cars," *SAE Int. J. Advances & Curr. Prac. in*

396 *Mobility* 1(3):1084-1099, 2019.

397 [2] Yang F, Yao C, Wang J, Ouyang M. "Load expansion of a dieseline compression ignition engine

398 with multi-mode combustion". *Fuel* 2016;171:5‑17.

399 [3] Vakiti, K., Deussen, J., Pilger, C., Nanjundaswamy, H., Szailer, T., Franke, M., Tomazic, D., Thomas,

400 K., Romijn, M., Deppenkemper, K., and Vagnoni, G. "In-Use Compliance Opportunity for Diesel

401 Powertrains," SAE Technical Paper 2018-01-0877, 2018.

402 [4] Boccardo, G., F. Millo, A. Piano, L. Arnone, S. Manelli, Simon Fagg, P. Gatti, Olaf E. Herrmann,

403 Dirk Queck and Jost Weber. "Experimental investigation on a 3000 bar fuel injection system for a SCR-

404 free non-road diesel engine." *Fuel* 243 (2019): 342-351.

405 [5] Niculae AL, Chiriac R, Racovitza A. Effects of Injection Rate Shape on Performance and Emissions

406 of a Diesel Engine Fuelled by Diesel and Biodiesel B20. *Applied Sciences*. 2022; 12(3):1333.

407 https://doi.org/10.3390/app12031333

408 [6] Kang, S., Lee, S., Hong, D., & Bae, C. (2022). Effects of Nozzle Orifice Diameter and Hole Number

409 on Diesel Combustion and Engine Performance. *International Journal of Automotive Technology, 23*,

410 481-494.

411 [7] Liu, H., Ma Jun-sheng, F. Dong, Y. Yang, X. Liu, Ma Gui-xiang, Z. Zheng and M. Yao.

412 "Experimental investigation of the effects of diesel fuel properties on combustion and emissions on a

413 multi-cylinder heavy-duty diesel engine." *Energy Conversion and Management* 171 (2018): 1787-1800.

414 [8] Ma, Y., L. Cui, X. Ma and J. Wang. "Optical study on spray combustion characteristics of

415 PODE/diesel blends in different ambient conditions." *Fuel* 272 (2020): 117691.

416 [9] Ferrari, A., C. Novara, E. Paolucci, O. Vento, M. Violante and T. Zhang. "A new closed-loop control

417 of the injected mass for a full exploitation of digital and continuous injection-rate shaping." *Energy*

418 *Conversion and Management* 177 (2018): 629-639.

419 [10] Zhai, C., Jin, Y., Wu, Q., Nishida, K., & Ogata, Y. (2021). Diesel spray and combustion of multi-

420 hole injectors with micro-hole under ultra-high injection pressure – Combustion characteristics. *Fuel,*

421 *300*, 120949.

422 [11] Wang, Xiangang, Zuohua Huang, W. Zhang, O. Kuti and K. Nishida. "Effects of ultra-high injection

423 pressure and micro-hole nozzle on flame structure and soot formation of impinging diesel spray." *Applied*

424 *Energy* 88 (2011): 1620-1628.

425 [12] Moon, S., Y. Gao, S. H. Park, J. Wang, N. Kurimoto and Y. Nishijima. "Effect of the number and

426 position of nozzle holes on in- and near-nozzle dynamic characteristics of diesel injection." *Fuel* 150

427 (2015): 112-122.

428 [13] Cavicchi, A., Postrioti, L., Pesce, F.C., and Ferrara, U., "Experimental Analysis of Fuel and

429 Injector Body Temperature Effect on the Hydraulic Behavior of Latest Generation Common Rail

430 Injection Systems," SAE Technical Paper 2018-01-0282, 2018, doi:10.4271/2018-01-0282.

431 [14] Kubota, Masaru, K. Yoshida, H. Shoji and H. Tanaka. "8 A Study of the Influence of Fuel

432 Temperature on Emission Characteristics and Engine Performance of Compression Ignition Engine."

433 SAE Technical Paper. (2002).

434 [15] Guangxin, Gao, Y. Zhu-lin, Zhou Apeng, Liu Sheng-hua and Wei Yanju. "Effects of Fuel

435 Temperature on Injection Process and Combustion of Dimethyl Ether Engine." *Journal of energy*

436 *resources technology* 135 4 (2013): 422021-422025 .

[16] Babadi, M. N., S. Kheradmand and C. Bae. "Experimental and Computational Investigation of Diesel and Gasoline Injection in a Direct Injection Compression Ignition Engine." *International Journal of Automotive Technology* 21 (2020): 23-32.

[17] Mamat, R., Abdullah, N. R., Xu, H., Wyszynski, M. L., & Tsolakis, A. (2009). *Effect of fuel temperature on performance and emissions of a common rail diesel engine operating with rapeseed methyl ester (RME)* (No. 2009-01-1896). SAE Technical Paper.

[18] Anis, Samsudin and Galuh Nur Budiandono. "Investigation of the effects of preheating temperature of biodiesel-diesel fuel blends on spray characteristics and injection pump performances." *Renewable Energy* 140 (2019): 274-280.

[19] El-Sharkawy, A., "Transient Thermal Analysis of Diesel Fuel Systems," *SAE Int. J. Mater. Manf.* 5(2):2012, doi:10.4271/2012-01-1049.

[20] A. Ferrari, Z. Jin, O. Vento, T. Zhang. An injected quantity estimation technique based on time–frequency analysis. Control Eng Pract, 116 (2021), 104910

[21] Catania, A., Ferrari, A., Manno, M., and Spessa, E., "Thermal Effect Simulation in High-Pressure Injection System Transient Flows," SAE Technical Paper 2004-01-0532, 2004.

[22] Payri, R., Salvador, F.J., Carreres, M., and Belmar-Gil, M., "An Investigation on the Fuel Temperature Variations Along a Solenoid Operated Common-Rail Ballistic Injector by Means of an Adiabatic 1D Model," SAE Technical Paper 2018-01-0275, 2018.

[23] Salvador, F., J. Gimeno, M. Carreres and M. Crialesi-Esposito. "Experimental assessment of the fuel heating and the validity of the assumption of adiabatic flow through the internal orifices of a diesel injector." *Fuel* 188 (2017): 442-451.

[24] Armas, O., S. Martínez-Martínez, C. Mata and C. Pacheco. "Alternative method for bulk modulus estimation of Diesel fuels." *Fuel* 167 (2016): 199-207.

[25] Ferrari, A. and Zhang T. "Influence of the injector setup on digital and continuous injection rate-shaping performance in diesel engine passenger cars." *Energy Conversion and Management* 205 (2020): 112259.

[26] Kim, J., J. Lee and K. Kim. "Numerical study on the effects of fuel viscosity and density on the injection rate performance of a solenoid diesel injector based on AMESim." *Fuel* 256 (2019): 115912.

[27] Salvador, F., M. Carreres, J. D. L. Morena and E. Martínez-Miracle. "Computational assessment of temperature variations through calibrated orifices subjected to high pressure drops: Application to diesel injection nozzles." *Energy Conversion and Management* 171 (2018): 438-451.

[28] Ferrari, A., C. Novara, O. Vento, M. Violante and T. Zhang. "A novel fuel injected mass feedback-control for single and multiple injections in direct injection systems for CI engines" *Fuel,* 334 (2023): 126670

[29] Postrioti, L., Giacomo Buitoni, F. Pesce and C. Ciaravino. "Zeuch method-based injection rate analysis of a common-rail system operated with advanced injection strategies." *Fuel* 128 (2014): 188-198.

[30] Bejan, Adrian. *Advanced engineering thermodynamics*. John Wiley & Sons, New York, 2016.

[31] Ferrari, A., C. Novara, E. Paolucci, O. Vento, M. Violante and T. Zhang. "Design and rapid prototyping of a closed-loop control strategy of the injected mass for the reduction of CO_2, combustion noise and pollutant emissions in diesel engines." *Applied Energy* 232 (2018): 358-367.

[32] Ferrari, A. and O. Vento. "Influence of Frequency-Dependent Friction Modeling on the Simulation of Transient Flows in High-Pressure Flow Pipelines." Journal of Fluids Engineering-transactions of The Asme 142 (2020).

[33] Catania, A.E., Ferrari, A. and Manno, M., 2009, "Development and Application of a Complete Multijet Common-Rail Injection-System Mathematical Model for Hydrodynamic Analysis and Diagnostics", *ASME J Eng. Gas Turb. Power*, 130(6), pp. 062809-1:13.

[34] Jin, Z., Vento, O., Zhang, T., Ferrari, A., Mittica, A., Ouyang, L., and Tan, S. (March 4, 2021). "Numerical-Experimental Optimization of the Common-Feeding Injection System Concept for Application to Light-Duty Commercial Vehicles." ASME. *J. Energy Resour. Technol*. December 2021; 143(12): 122304. https://doi.org/10.1115/1.4050133

[35] Blackburn JF, Reethof G, Shearer JL. "Fluid power control". MIT Press; 1960.

[36] Payri, R., F. Salvador, M. Carreres and J. D. L. Morena. "Fuel temperature influence on the performance of a last generation common-rail diesel ballistic injector. Part II: 1D model development, validation and analysis." *Energy Conversion and Management* 114 (2016): 376-391.

492   [37] Ferrari, A.. "Fluid dynamics of acoustic and hydrodynamic cavitation in hydraulic power

493   systems." *Proceedings of the Royal Society A: Mathematical, Physical and Engineering Sciences* 473

494   (2017).

495   [38] McCloy, D. and H. Martin. "Control of Fluid Power : Analysis and design", 2nd edition. Ellis

496   Horwood Limited 1980.

497   [39] Nurick WH. 1976, "Orifice cavitation and its effect on spray mixing." J. Fluids Eng. 98, 681–689.

498   [40] Payri, R., J. M. García, F. Salvador and J. Gimeno. "Using spray momentum flux measurements to

499   understand the influence of diesel nozzle geometry on spray characteristics." *Fuel* 84 (2005): 551-561.

500   [41] Zhao, Jianhui, L. Grekhov and Peng-fei Yue. "Limit of Fuel Injection Rate in the Common Rail

501   System under Ultra-High Pressures." *International Journal of Automotive Technology* 21 (2020): 649-

502   656.